International Journal of Solids and Structures 47 (2010) 1350–1360

Contents lists available at ScienceDirect

International Journal of Solids and Structures

journal homepage: www.elsevier.com/locate/ijsolstr

Nonlocal regularisation of a model based on breakage mechanics for granular materials

Giang D. Nguyen *, Itai Einav

School of Civil Engineering, The University of Sydney, Sydney, NSW 2006, Australia

ARTICLE INFO

Article history:
Received 4 March 2009
Received in revised form 17 January 2010
Available online 25 January 2010

Keywords:
Breakage mechanics
Granular material
Nonlocal
Crushing
Length scale

ABSTRACT

We apply a nonlocal regularisation method to a breakage model recently proposed for the constitutive modelling of crushable granular materials. Coupling between material points is taken into account through the nonlocal averaging applied to the yield function. This enables us to introduce a length scale to continuum breakage models, and therefore helps to overcome numerical difficulties arising from physical instabilities encountered when the material effectively undergoes softening due to crushing. The numerical implementation of the nonlocal version of a breakage model is briefly presented. To demonstrate its promising features, this nonlocal model is used in a series of numerical analyses of high pressure shearing processes, in which grain crushing mechanism governs the material behaviour.

1. Introduction

Careful construction of constitutive models that consider essential microscopic mechanisms can explain experimentally observed features of material behaviour through physical arguments. In return, such models are typically advantageous for the numerical analysis of engineering problems, since these may extend to situations that are beyond the experimental phenomenology. The recent theory of breakage mechanics (Einav, 2007a,b) enables to construct constitutive models that account for the microscopic details of grain crushing. Consequently, models of this theory have been applied successfully in the numerical analysis of various geomechanical and geophysical problems where grain crushing plays an important role, e.g. landslides (Nguyen et al., 2008) and high pressure cataclastic shear (Einav and Nguyen, 2009).

Material stability is an issue one should always deal with when developing constitutive models for softening materials. In crushable granular materials, the crushing of particles in confined conditions leads to softening behaviour observed at the macro scale. We assume here that there are no other types of instability caused by inadequate treatments of boundary conditions or initial conditions. Therefore, within the framework of continuum mechanics, material softening from the loss of positive definiteness of the stiffness tensor is the cause of numerical issues that can arise when one tries to analyse a complete boundary value problem (BVP) using local (conventional) constitutive models without a length scale. Mathematically, due to this loss of material stability, the governing differential equations of continuum mechanics will lose its ellipticity (in statics) or hyperbolicity (in dynamics). As a consequence, the continuum modelling of solids/structures made of softening material leads to ill-posed BVPs (Jirásek and Bazant, 2002). In numerical analysis, this ill-posedness leads to the localisation of deformation into a narrow band, the width of which is governed by the resolution of the spatial discretisation. Outside this localisation band, the material is unloaded elastically. The total energy dissipation (i.e., the sum of material dissipation inside the localisation band) therefore reduces with refinement of the spatial discretisation. In the limit, once the element size (e.g. in finite element analysis) approaches zero, the numerical results converge to a solution with zero localisation band size and zero total dissipation. This numerical prediction is physically unrealistic and is due to the inadequacy of conventional continuum mechanics to deal with ill-posed BVPs. The resolution of the above-mentioned problems requires a regularisation through the introduction of a length scale to the material model. In continuum modelling of softening (granular) materials the regularisation can be as simple as possible utilizing the concept of smeared crack/deformation (e.g. Crook et al., 2006) or more sophisticated using micro-polar (Tejchman, 2004a,b; Tejchman and Gorski, 2008) or nonlocal theories (Marcher and Vermeer, 2001; Maier, 2003, 2004; Tejchman, 2004a,b).

Once a particle is broken into smaller fragments, within a granular volume element, its collapse not only induces sudden movements of neighbouring particles, but also leads to the redistribution/transmission of elastically stored and kinetic energies within a certain volume of the material (Nguyen and Einav, 2009a). This highlights the notion of long range interactions between particles, which introduce effects that the classical equilib-

* Corresponding author. Tel.: +61 2 9351 3721; fax: +61 2 9351 3343.
E-mail addresses: giang.nguyen@trinity.oxon.org, giang.nguyen@sydney.edu.au (G.D. Nguyen).

0020-7683/$ - see front matter © 2010 Elsevier Ltd. All rights reserved.
doi:10.1016/j.ijsolstr.2010.01.020

rium equations of conventional continuum mechanics might not be able to capture. Even without grain crushing effects, numerical analysis of granular materials based on the discrete element method (Ord et al., 2007) also indicated the presence of long range interaction effects, which cannot be captured using conventional continuum modelling. The requirement to take into account the long range interactions in granular materials motivates the development of nonlocal approach to the modelling of crushable granular materials.

In a rational way, an intrinsic length scale of a nonlocal continuum material model should ideally emerge from upscaling microstructural details. In granular materials, where particle crushing plays the role of the governing micro-structural mechanism, the induced effects should be linked with the length scale that is associated with the long range correlations. In the constitutive modelling, this link is useful in determining parameters of nonlocal model, which involves both the spatial parameters in charge of the interaction between material points and the local parameters that control the pointwise response of a material point. In this study, we avoid entering such an interpretation of the upscaling process; we view the nonlocal regularisation simply as a numerical mean to eliminate unwanted stability issues that existing local constitutive models may encounter. In particular, we adapt a nonlocal regularisation technique and apply it directly to the nonlocal averaging of the yield function of an existing (local) breakage model (Einav, 2007a,b).

The paper is organized as follows. The formulation of the local breakage model will be briefly presented in the next section, following early developments in Einav (2007a,b,c), and focusing on the simplest approach based on linear elasticity. This is then succeeded by the nonlocal regularisation applying to a rearranged form of the breakage/yield criterion, and then the description of a stress return algorithm for nonlocal incremental constitutive equations. We highlight the role of the particular choice of the loading function in the success of the nonlocal regularisation technique. In the case of the breakage model adopted in this study, it is not sufficient to consider as nonlocal only quantities directly controlling the softening process, as suggested in early work on nonlocal damage model by Pijaudier-Cabot and Bazant (1987). The numerical illustrations in the following section demonstrate how nonlocal regularisation can eliminate the mesh-dependence encountered in predictions by local models. We note that these results are only intended to show numerically the effectiveness of the regularisation. More rigorous localisation analysis (e.g. the dispersion analysis by Pijaudier-Cabot and Benallal (1993), Sluys et al. (1993), Borino et al. (2003) is to be covered in a forthcoming paper. In the conclusion, we discuss how the nonlocal regularisation of breakage models can be useful to solving geotechnical/geophysical problems.

2. A local breakage model

We start with the formulation of a local breakage model based on early developments in Einav (2007a,b). We then set up a starting point for introducing a nonlocal regularisation technique which could be applicable to such a model. Standard notations in soil mechanics are used: mean effective stress p, shear stress q, total volumetric strain ε_v and elastic volumetric strain ε_v^e, total shear strain ε_s and elastic shear strain ε_s^e. The energy potential Ψ and dissipation potential Φ are assumed to take the following forms (Einav, 2007c):

$$\Psi = \frac{1}{2}(1-\vartheta B)\left(K\varepsilon_v^{e^2} + 3G\varepsilon_s^{e^2}\right) \tag{1}$$

$$\Phi = \sqrt{\Phi_B^2 + \Phi_p^{v^2} + \Phi_p^{s^2}} \tag{2}$$

in which B is the scalar breakage variable; ϑ is the index property measuring how far the initial *gsd* (grain size distribution) is from the ultimate *gsd* (Einav, 2007a) through second order moments of these distributions; K and G are the bulk and shear modulii, respectively. A more complicated form of the energy potential taking into account the pressure-dependency of the elastic behaviour can be found in Nguyen and Einav (2009a).

In the above we highlight that the Helmholtz free energy potential is specifically formulated in terms of elastic strains and not in terms of the total strain minus the plastic strain. This is consistent with the work of Rubin (2001), who motivates the physical reasons why "constitutive equations must depend on state variables that, in principle, can be measured without any prior knowledge of the past history of deformation of the material. Within the context of this notion of state, elastic strain is a state variable, whereas the total strain and plastic strains are not state variables since they are measured with respect to an arbitrary reference configuration". In the line of this proposition, the dissipation potential can only be a function of the rate of plastic deformation rather than its cumulative value. Furthermore, the proposition above does not require the acceptance of the assumption on the decomposition of total strain into plastic and elastic strains in additive form. The notion of elastic–plastic decomposition can only be valid in its incremental form (see Collins and Einav, 2005). Similar to the damage mechanics theory of solid-like materials the breakage mechanics theory of brittle granular materials also deals with permanent micro-structural fabric alterations, and creation of new surface area. However, these theories are fundamentally different, as they deal with totally distinguishable materials. The mathematical differences initiate from the dissimilar definition of the internal variables, i.e., breakage B in breakage mechanics (Einav, 2007a) and damage D in damage mechanics (e.g. Lemaitre, 1992). The breakage, B, weighs the relative distance of a current *gsd* $g(x)$ from an initial and ultimate *gsd*'s $g_0(x)$ and $g_u(x)$, via the relation:

$$g(x) = g_0(x)(1-B) + g_u(x)B \tag{3}$$

On the other hand, in damage mechanics, the effect of micro-voids or micro-crack openings on the solid behaviour is accounted for through a directional damage variable $D = A_v/A$, where A_v is the void area and A the total cross sectional area with normal vector $\mathbf{n}$ of a representative volume element (RVE). Furthermore, while the general mathematical structure of the Helmholtz energy potentials in both theories may seem related, these are derived from entirely different physical arguments. In particular, in the simplest form of damage mechanics, where a uniform distribution of voids/micro-cracks within a RVE is assumed, D becomes a scalar variable, and the corresponding Helmholtz free energy includes the multiplication of the term $(1-D)$ by the potential energy of an 'un-damaged' continuum. This structure is the outcome of the strain equivalence principle (Lemaitre, 1971). On the other hand, in breakage mechanics, the term $(1-\vartheta B)$ appears instead of the $(1-D)$ term and multiplies the strain energy in a reference particle size. The term $(1-\vartheta B)$ emerges from a statistical homogenization operation via the *gsd* of Eq. (3), and the universal scaling of the stored energy in the particles with their surface area (Einav, 2007a); the index property ϑ is a signature of this operation.

In Eq. (2), the dissipation potential Φ comprises three parts corresponding to breakage dissipation Φ_B, plastic volumetric dissipation Φ_p^v and plastic shear dissipation Φ_p^s (Einav, 2007b):

$$\Phi_B = \frac{\sqrt{E_B E_c}}{(1-B)\cos\omega}\delta B \tag{4}$$

$$\Phi_p^v = \frac{p}{(1-B)\sin\omega}\sqrt{\frac{E_c}{E_B}}\delta\varepsilon_v^p \tag{5}$$

$$\Phi_p^s = Mp|\delta\varepsilon_s^p| \tag{6}$$

Coupling between grain crushing and plastic volumetric deformation is taken through the coupling angle ω; parameter $M = q_u/p_u$ is the ratio between the ultimate shear stress q_u and ultimate volumetric stress p_u at failure; the energy threshold E_c in Eqs. (4) and (5) is related to the crushing pressure p_c in isotropic compression through the relationship: $p_c = \sqrt{2KE_c/\vartheta}$ (Einav, 2007c). An elaborate discussion on the roles of each components of the dissipation potential can be found in Nguyen and Einav (2009a).

The model formulation follows thermo-mechanical procedures established by Ziegler (1983) for rate-independent elastoplastic models, considering the notions of breakage and coupled dissipations. In particular, the generalised stresses (7)–(9) and the dissipative generalised stresses (10)–(12) are distinguished, which adds formal advantages as discussed by Houlsby and Puzrin (2000). From the energy potential, the triaxial stresses (p, q) and breakage energy E_B – the conjugated thermodynamic forces of the triaxial strains $(\varepsilon_v^e, \varepsilon_s^e)$ and breakage variable B, respectively – are:

$$p = \frac{\partial \Psi}{\partial \varepsilon_v^e} = (1 - \vartheta B) K \varepsilon_v^e \tag{7}$$

$$q = \frac{\partial \Psi}{\partial \varepsilon_s^e} = 3(1 - \vartheta B) G \varepsilon_s^e \tag{8}$$

$$E_B = -\frac{\partial \Psi}{\partial B} = \frac{\vartheta}{2}\left(K\varepsilon_v^{e^2} + 3G\varepsilon_s^{e^2}\right) \tag{9}$$

In a similar way, the dissipative stresses $(\bar{p}, \bar{q})$ and dissipative breakage energy $\bar{E}_B$ are obtained from the dissipation potential as:

$$\bar{p} = \frac{\partial \Phi}{\partial \delta\varepsilon_v^p} = \frac{\partial \Phi}{\partial \Phi_p^v}\frac{\partial \Phi_p^v}{\partial \delta\varepsilon_v^p} = \frac{\Phi_p^v}{\sqrt{\Phi_B^2 + \Phi_p^{v^2} + \Phi_p^{s^2}}}\frac{\partial \Phi_p^v}{\partial \delta\varepsilon_v^p} \tag{10}$$

$$\bar{q} = \frac{\partial \Phi}{\partial \delta\varepsilon_s^p} = \frac{\partial \Phi}{\partial \Phi_p^s}\frac{\partial \Phi_p^s}{\partial \delta\varepsilon_s^p} = \frac{\Phi_p^s}{\sqrt{\Phi_B^2 + \Phi_p^{v^2} + \Phi_p^{s^2}}}\frac{\partial \Phi_p^s}{\partial \delta\varepsilon_s^p} \tag{11}$$

$$\bar{E}_B = \frac{\partial \Phi}{\partial \delta B} = \frac{\partial \Phi}{\partial \Phi_B}\frac{\partial \Phi_B}{\partial \delta\varepsilon_B} = \frac{\Phi_B}{\sqrt{\Phi_B^2 + \Phi_p^{v^2} + \Phi_p^{s^2}}}\frac{\partial \Phi_B}{\partial \delta\varepsilon_B} \tag{12}$$

For rate-independent processes, the yield function y^* in generalised stress space is obtained as a result of the degenerate Legendre transformation of the dissipation potential (2), given that the dissipation potential and its components are homogeneous first order in the rates of internal variables:

$$y^* = \left(\frac{\bar{E}_B}{\partial \Phi_B/\partial \delta B}\right)^2 + \left(\frac{\bar{p}}{\partial \Phi_p^v/\partial \delta\varepsilon_v^p}\right)^2 + \left(\frac{\bar{q}}{\partial \Phi_p^s/\partial \delta\varepsilon_s^p}\right)^2 - 1 \leqslant 0 \tag{13}$$

From the above yield function, the following flow rules ($\delta\lambda$ is a non-negative multiplier) are obtained:

$$\delta B = \delta\lambda \frac{\partial y^*}{\partial \bar{E}_B} = 2\delta\lambda \frac{\bar{E}_B}{(\partial \Phi_B/\partial \delta B)^2} = 2\delta\lambda \frac{\bar{E}_B (1-B)^2 \cos^2\omega}{E_B E_c} \tag{14}$$

$$\delta\varepsilon_v^p = \delta\lambda \frac{\partial y^*}{\partial \bar{p}} = 2\delta\lambda \frac{\bar{p}}{\left(\partial \Phi_p^v/\partial \delta\varepsilon_v^p\right)^2} = 2\delta\lambda \frac{\bar{p} E_B (1-B)^2 \sin^2\omega}{p^2 E_c} \tag{15}$$

$$\delta\varepsilon_s^p = \delta\lambda \frac{\partial y^*}{\partial \bar{q}} = 2\delta\lambda \frac{\bar{q}}{\left(\partial \Phi_p^s/\partial \delta\varepsilon_s^p\right)^2} = 2\delta\lambda \frac{\bar{q}}{M^2 p^2} \tag{16}$$

Using the orthogonality condition (Ziegler, 1983) in the form $p = \bar{p}, q = \bar{q}$ and $E_B = \bar{E}_B$ we can rewrite the flow rules as:

$$\delta B = 2\delta\lambda \frac{(1-B)^2 \cos^2\omega}{E_c} \tag{17}$$

$$\delta\varepsilon_v^p = 2\delta\lambda \frac{E_B (1-B)^2 \sin^2\omega}{p E_c} \tag{18}$$

$$\delta\varepsilon_s^p = 2\delta\lambda \frac{q}{M^2 p^2} \tag{19}$$

The breakage/yield function, denoted here as y in mixed stress-energy space, can be rewritten using the orthogonality condition, along with Eqs. (4)–(6):

$$y = \frac{E_B (1-B)^2}{E_c} + \left(\frac{q}{Mp}\right)^2 - 1 \leqslant 0 \tag{20}$$

In true stress space, using (7)–(9) we can rewrite the breakage energy E_B in terms of stress, as:

$$E_B = \frac{\vartheta}{2(1-\vartheta B)^2}\left(\frac{p^2}{K} + \frac{q^2}{3G}\right) \tag{21}$$

Then the yield function can be rewritten in triaxial stress space as:

$$y = \frac{\vartheta}{2E_c}\left(\frac{p^2}{K} + \frac{q^2}{3G}\right)\left(\frac{1-B}{1-\vartheta B}\right)^2 + \left(\frac{q}{Mp}\right)^2 - 1 \leqslant 0 \tag{22}$$

3. Nonlocal regularisation

Softening behaviour is well known in the literature as the cause of instabilities and is observed in many geotechnical problems. Although these instabilities are often physical, some non-physical irregularities may emerge when solving the corresponding BVPs using conventional continuum mechanics, due to the ill-posedness of these BVPs. A review on instability and bifurcation due to material softening has been documented in the literature (e.g. Neilsen and Schreyer, 1993). Without enhancements (via regularisation techniques), either to the equilibrium equations or to the constitutive model, the numerical simulations of problems involving material softening usually result in discretisation-dependent solutions (e.g. as later demonstrated in Fig. 4a, using the local model of the previous section). Various regularisation methods have been proposed and used effectively in the literature, including using viscosity and/or nonlocal enhancement to the constitutive modelling. In this study, nonlocal regularisation of integral type is adopted for the local breakage model of the preceding section.

We recall the local breakage/yield criterion in Eq. (20). The way nonlocality is introduced to the constitutive equations is important, as illustrated in a paper by Jirásek (1998), in which different nonlocal treatments to a simple damage model were explored. Inappropriate treatment of nonlocal variable/quantity can lead to bad features of the nonlocal model (e.g. non-uniqueness and/or instability of the numerical analysis).

Since breakage is the active mechanism governing the dissipative process (Einav, 2007b) that leads to softening, a rational way to regularise the constitutive model is to apply nonlocality to the breakage energy E_B (21), the thermodynamic conjugate to the breakage variable B. This is similar to the use of nonlocal damage energy in the pioneering work by Pijaudier-Cabot and Bazant (1987). In addition, the presence of plastic strain increments in the constitutive model as a passive dissipation mechanism (Einav, 2007b), the additional nonlocal treatments to the thermodynamic forces (triaxial stresses p and q in our model) associated with the elastic volumetric and shear strains can be seen rational. These nonlocal enhancements however did not act as good localisation limiters, and convergence to a unique solution upon refining the discretisation could not be achieved.

From the yield function (20), it can be seen that the second term involving shear stress q becomes dominant when breakage B approaches unity. Therefore applying nonlocality only to the breakage energy E_B (or either, to the first term of the yield function) was experienced not to help prevent localisation into infinitesimal zone in problems involving shearing. Furthermore, numerical experiments showed that applying nonlocal treatment to all quantities (E_B, p and q) controlling the model response, in the form

$$y = \frac{\widehat{E}_B(1-B)^2}{E_c} + \left(\frac{\hat{q}}{M\hat{p}}\right)^2 - 1 \leqslant 0$$

or to the whole yield function (20) also did not help prevent the localisation. This is because the yield function in its current form (20) was normalized to compare to one, which gradually neutralises the effects of nonlocal terms $\widehat{E}_B$, $\hat{p}$ and $\hat{q}$ (or $\widehat{C}$, where $C = E_B(1-B)^2/E_c + q^2/(Mp)^2$) when breakage B is growing. In other words, the nonlocal effect is gradually vanishing with increasing breakage B. Further details on this can be found in our recent paper (Nguyen and Einav, in press).

In this paper we adopt the following treatment, using a slight rearrangement of the yield function, leading to a possible useful mathematical form of the yield function:

$$y = \frac{E_B}{E_c} + \left(\frac{q}{Mp(1-B)}\right)^2 - \frac{1}{(1-B)^2} \leqslant 0 \tag{23}$$

The nonlocal breakage/yield function, written for a material point at point $\mathbf{x}$ and accounting for the behaviour at several neighbouring point $\mathbf{y}$ (Fig. 1), is then:

$$y(\mathbf{x}) = \widehat{C}(\mathbf{x}) - \frac{1}{(1-B(\mathbf{x}))^2} \leqslant 0 \tag{24}$$

where

$$\widehat{C}(\mathbf{x}) = \frac{1}{G(\mathbf{x})}\int_{V_d} g(\|\mathbf{y}-\mathbf{x}\|)C(\mathbf{y})dV(\mathbf{y}) \tag{25}$$

and $C = \frac{E_B}{E_c} + (\frac{q}{Mp(1-B)})^2$

In the above expression V_d is the volume where the nonlocal averaging takes place; it is dependent on the selected type of weighting function $g(\|\mathbf{y}-\mathbf{x}\|) \geqslant 0$, e.g. Gaussian or bell-shaped distributions; and $G(\mathbf{x})$ is defined as a weight associated with the material point $\mathbf{x}$, aiming at normalizing the weighting scheme:

$$G(\mathbf{x}) = \int_{V_d} g(\|\mathbf{x}-\mathbf{y}\|)dV(\mathbf{y}) \tag{26}$$

The flow rules of the model retain their local forms (17)–(19). The stress update algorithm for the numerical implementation of this nonlocal model will be presented in the next section.

4. Numerical implementation

The numerical implementation of the above nonlocal breakage model is briefly presented for finite element analyses. The tensorial form of the triaxial model described in Section 2 is used. Following standard definitions, the triaxial stresses and strains are written in terms of the stress and strain invariants:

$$p = -\frac{1}{3}tr(\boldsymbol{\sigma}); \quad q = \sqrt{\frac{3}{2}\mathbf{s}:\mathbf{s}}; \quad \varepsilon_v = tr(\boldsymbol{\varepsilon}); \quad \varepsilon_s = \sqrt{\frac{2}{3}\mathbf{e}:\mathbf{e}} \tag{27}$$

where $\mathbf{s} = \boldsymbol{\sigma} - \boldsymbol{\delta}tr(\boldsymbol{\sigma})/3$; and

$$\mathbf{e} = \boldsymbol{\varepsilon} - \boldsymbol{\delta}tr(\boldsymbol{\varepsilon})/3 (\boldsymbol{\delta} \text{ is the Kronecker delta}) \tag{28}$$

From the energy potential (1), we obtain the relationship between stress, strain and breakage in tensorial form as:

$$\boldsymbol{\sigma} = \frac{\partial \Psi}{\partial \boldsymbol{\varepsilon}} = (1-\vartheta B)\mathbf{D} : (\boldsymbol{\varepsilon} - \boldsymbol{\varepsilon}^p) \tag{29}$$

where $\mathbf{D}$ is the linear elastic stiffness tensor.

The flow rules (17)–(19) in general stress space are:

$$\begin{aligned}\delta\boldsymbol{\varepsilon}^p &= \delta\lambda\frac{\partial y^*}{\partial \boldsymbol{\sigma}} = \delta\lambda\left(\frac{\partial y^*}{\partial p}\frac{\partial p}{\partial \boldsymbol{\sigma}} + \frac{\partial y^*}{\partial q}\frac{\partial q}{\partial \boldsymbol{\sigma}}\right)\\ &= \delta\lambda\left(2\frac{(1-B)^2E_B\sin^2\omega}{pE_c}\frac{\boldsymbol{\delta}}{3} + \frac{3\mathbf{s}}{M^2p^2}\right)\end{aligned} \tag{30}$$

and

$$\delta B = \delta\lambda\frac{\partial y^*}{\partial E_B} = 2\delta\lambda\frac{(1-B)^2\cos^2\omega}{E_c} \tag{31}$$

which give us the ratio $\mathbf{Q}$ between the increments of plastic strain tensor and breakage as:

$$\mathbf{Q} = \frac{\delta\boldsymbol{\varepsilon}^p}{\delta B} = \frac{E_B\tan^2\omega}{p}\frac{\boldsymbol{\delta}}{3} + \frac{3\mathbf{s}}{M^2p^2}\frac{E_c}{2(1-B)^2\cos^2\omega} \tag{32}$$

We now turn attention to the spatial discretisation followed by the temporal linearization of the nonlocal yield function (24). For the spatial discretisation, with the presence of the nonlocal averaging involving material points neighbouring to the considered material point, the same finite element discretisation is used, as that for the BVP. From Eq. (25), the discretisation using the finite element method leads to:

$$\widehat{C}(\mathbf{x}) = \frac{\sum_{e=1}^{n}\int_{\mathbf{y}\in V_e} g(\|\mathbf{y}-\mathbf{x}\|)C(\mathbf{y})dV(\mathbf{y})}{\sum_{e=1}^{n}\int_{\mathbf{y}\in V_e} g(\|\mathbf{x}-\mathbf{y}\|)dV(\mathbf{y})} \tag{33}$$

where V_e denotes the volume of element e and n is the total number of elements inside the interaction volume V_d defined by a sphere centred at $\mathbf{x}$ and with radius R. Using the same integration rule as that of the finite element discretisation, we can rewrite (33) as:

$$\widehat{C}(\mathbf{x}_i) = \frac{\sum_{e=1}^{n}\sum_{j=1}^{m_e}\omega_j^e g\left(\|\mathbf{y}_j^e - \mathbf{x}_i\|\right)\det\mathbf{J}_j^e C\left(\mathbf{y}_j^e\right)}{\sum_{e=1}^{n}\sum_{j=1}^{m_e}\omega_j^e g\left(\|\mathbf{y}_j^e - \mathbf{x}_i\|\right)\det\mathbf{J}_j^e} \tag{34}$$

in which i is the integration point under consideration, j is the jth Gauss point of element e; m_e is the number of Gauss points of this

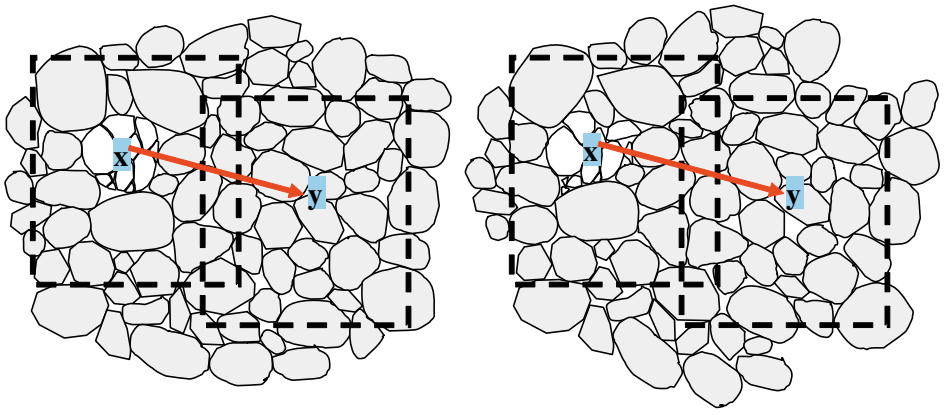

Fig. 1. Schematic view of the nonlocal interaction between points $\mathbf{x}$ and $\mathbf{y}$ in a grain crushing event.

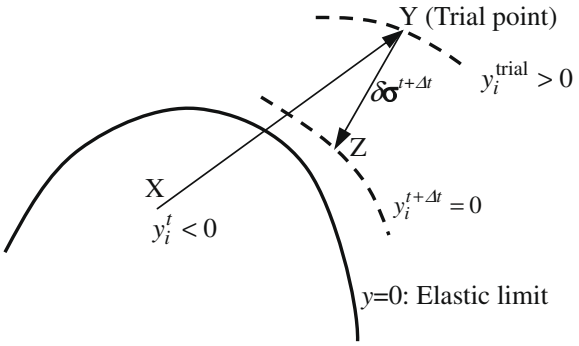

Fig. 2. Pictorial presentation of the stress return algorithm (after Crisfield, 1997).

element inside the interaction volume; ω_j^e and $\mathbf{J}_j^e$ are, respectively, the weight and Jacobian matrix at Gauss point j of element e. The above expression can be rewritten in compact form as:

$$\widehat{C}_i = \sum_j^{n_i} w_{ij} C_j \tag{35}$$

where n_i is the total number of Gauss points inside the nonlocal interaction volume at point i, and the weight w_{ij} for the interaction between material points i and j is in the form:

$$w_{ij} = \frac{\omega_j^e g\left(\|\mathbf{y}_j^e - \mathbf{x}_i\|\right) \det \mathbf{J}_j^e}{\sum_{e=1}^{n}\sum_{j=1}^{m_e} \omega_j^e g\left(\|\mathbf{y}_j^e - \mathbf{x}_i\|\right) \det \mathbf{J}_j^e} \tag{36}$$

The nonlocal yield function (24) at integration point i can then be written in a spatially discretised form as:

$$y_i = \sum_j^{n_i} w_{ij} C_j - \frac{1}{(1-B_i)^2} \leqslant 0 \tag{37}$$

Performing a Taylor expansion of the yield function at the trial stress point (Fig. 2), we have (from now on the notation $\partial A_i/\partial x$ for $(\partial A/\partial x)|_i$, which means $\partial A/\partial x$ evaluated at integration point i, is adopted):

$$\begin{aligned} y_i^{t+\Delta t} &= y_i^{\text{trial}} + \sum_j^{n_i} w_{ij}\delta C_j - \frac{2\delta B_i}{(1-B_i)^3} \\ &= y_i^{\text{trial}} + \sum_j^{n_i} w_{ij}\left[\frac{\partial C_j}{\partial B}\delta B_j + \frac{\partial C_j}{\partial E_B}\delta E_{Bj} + \frac{\partial C_j}{\partial p}\delta p_j + \frac{\partial C_j}{\partial q}\delta q_j\right] \\ &\quad - \frac{2\delta B_i}{(1-B_i)^3} \end{aligned} \tag{38}$$

Expanding the linearized yield function using the chain rule results in:

$$\begin{aligned} y_i^{t+\Delta t} =& y_i^{\text{trial}} - \frac{2\delta B_i}{(1-B_i)^3} \\ &+ \sum_j^{n_i} w_{ij}\left[\frac{\partial C_j}{\partial E_B}\left(\frac{\partial E_{Bj}}{\partial B}\delta B_j + \frac{\partial E_{Bj}}{\partial p}\frac{\partial p_j}{\partial \boldsymbol{\sigma}} : \delta\boldsymbol{\sigma}_j + \frac{\partial E_{Bj}}{\partial q}\frac{\partial q_j}{\partial \boldsymbol{\sigma}} : \delta\boldsymbol{\sigma}_j\right)\right. \\ &\left. + \frac{\partial C_j}{\partial B}\delta B_j + \frac{\partial C_j}{\partial p}\frac{\partial p_j}{\partial \boldsymbol{\sigma}} : \delta\boldsymbol{\sigma}_j + \frac{\partial C_j}{\partial q}\frac{\partial q_j}{\partial \boldsymbol{\sigma}} : \delta\boldsymbol{\sigma}_j\right] \end{aligned} \tag{39}$$

Note that the corrective stress increment when going from trial stress point Y to the new stress point Z (Fig. 2) has the following form:

$$\delta\boldsymbol{\sigma}^{t+\Delta t} = \boldsymbol{\sigma}^{t+\Delta t} - \boldsymbol{\sigma}^{\text{trial}} = \left[-(1-\vartheta B)\mathbf{D} : \delta\boldsymbol{\varepsilon}^p - \frac{\vartheta\boldsymbol{\sigma}}{(1-\vartheta B)}\delta B\right]\Big|_{\text{trial}} \tag{40}$$

We note also that this corrective stress increment is evaluated at the trial stress point, so the subscript "trial" can be dropped out when substituting (40) into the expression (39) of the linearized yield/breakage function. Therefore we have (for simplicity, assuming ϑ is the same for the whole granular sample, e.g. homogeneous *gsd*):

$$\begin{aligned} y_i^{t+\Delta t} =& \sum_j^{n_i} w_{ij}\left\{\left(\frac{\partial C_j}{\partial B} + \frac{\partial C_j}{\partial E_B}\frac{\partial E_{Bj}}{\partial B}\right)\delta B_j - \left[\left(\frac{\partial C_j}{\partial E_B}\frac{\partial E_{Bj}}{\partial p} + \frac{\partial C_j}{\partial p}\right)\frac{\partial p_j}{\partial \boldsymbol{\sigma}}\right.\right. \\ &\left.\left. + \left(\frac{\partial C_j}{\partial E_B}\frac{\partial E_{Bj}}{\partial q} + \frac{\partial C_j}{\partial q}\right)\frac{\partial q_j}{\partial \boldsymbol{\sigma}}\right] : \left[(1-\vartheta B_j)\mathbf{D}_j : \delta\boldsymbol{\varepsilon}_j^p + \frac{\vartheta\boldsymbol{\sigma}_j\delta B_j}{(1-\vartheta B_j)}\right]\right\} \\ &+ y_i^{\text{trial}} - \frac{2\delta B_j}{(1-B_j)^3} \end{aligned} \tag{41}$$

Using the flow rules in the form (32), we can rewrite (41) as

$$\begin{aligned} y_i^{t+\Delta t} =& \sum_j^{n_i} w_{ij}\left\{\left(\frac{\partial C_j}{\partial B} + \frac{\partial C_j}{\partial E_B}\frac{\partial E_{Bj}}{\partial B}\right)\delta B_j - \left[\left(\frac{\partial C_j}{\partial E_B}\frac{\partial E_{Bj}}{\partial p} + \frac{\partial C_j}{\partial p}\right)\frac{\partial p_j}{\partial \boldsymbol{\sigma}}\right.\right. \\ &\left.\left. + \left(\frac{\partial C_j}{\partial E_B}\frac{\partial E_{Bj}}{\partial q} + \frac{\partial C_j}{\partial q}\right)\frac{\partial q_j}{\partial \boldsymbol{\sigma}}\right] : \left[(1-\vartheta B_j)\mathbf{D}_j : \mathbf{Q}_j + \frac{\vartheta\boldsymbol{\sigma}_j}{(1-\vartheta B_j)}\right]\delta B_j\right\} \\ &+ y_i^{\text{trial}} - \frac{2\delta B_i}{(1-B_i)^3} \end{aligned} \tag{42}$$

Or in simplified form

$$y_i^{t+\Delta t} = y_i^{\text{trial}} - \frac{2\delta B_i}{(1-B_i)^3} + \sum_j^{n_i} w_{ij} U_j \delta B_j \tag{43}$$

where

$$\begin{aligned} U =& \left(\frac{\partial C}{\partial B} + \frac{\partial C}{\partial E_B}\frac{\partial E_B}{\partial B}\right) \\ &- \left[\left(\frac{\partial C}{\partial E_B}\frac{\partial E_B}{\partial p} + \frac{\partial C}{\partial p}\right)\frac{\partial p}{\partial \boldsymbol{\sigma}} + \left(\frac{\partial C}{\partial E_B}\frac{\partial E_B}{\partial q} + \frac{\partial C}{\partial q}\right)\frac{\partial q}{\partial \boldsymbol{\sigma}}\right] \\ &: \left[(1-\vartheta B)\mathbf{D} : \mathbf{Q} + \frac{\vartheta\boldsymbol{\sigma}}{(1-\vartheta B)}\right] \end{aligned} \tag{44}$$

Note that Eq. (43) is written for all integration points undergoing grain crushing. These equations are coupled through the nonlocal averaging. Together, they form a system of linear algebraic equations which can be solved for breakage increments at any iteration of the incremental-iterative solution scheme based on the Newton–Raphson method. The corrective stress increments (40) at all crushed material points are then calculated using the breakage increments and flow rule in the form (32).

Due to nonlocality, it is impossible to perform the stress update pointwise. In the implementation, at first trial states of all integration points are reached by assuming the stress increments are elastic, using the secant elastic-breakage stiffness. Then the set of integration points potentially undergoing crushing is determined based on the sign of the yield/breakage criterion at their trial states. The system (43) is formed only for integration points having $y^{\text{trial}} > 0$. To enforce the satisfaction of the yield criterion (24) (within a given tolerance) at the end of the increment, a repetition of the same process is performed but with point Y replaced with Z, noting that there are no elastic stress increments in the subsequent iterations. During this iterative process, the set of integration points undergoing crushing are kept unchanged. This iterative process is also combined with sub-incrementation to improve the performance of the algorithm. In nonlocal numerical analysis, some yielded (integration) points can be unloaded elastically after a certain stage of loading. In other words, at the end of the stress update process certain integration points can encounter negative breakage increments. This means that the load increment might be too big and that those integration points might not be undergoing crushing. This situation is taken care of in the analysis by reverting to the last converged position and reducing the load increments.

The above stress return algorithm does not require the determination of the intersections between the stress increment vectors and the yield surfaces, which is impossible in the case of nonlocal constitutive equations. In other words, whether or not the material point has undergone crushing in the past is not important to the algorithm. On the other hand, the yield condition (24) is enforced in its total form at any iteration, thus helping to avoid the inaccuracies encountered when the consistency condition is applied. Further refinements of the algorithm and its performance can be found in Nguyen and Einav (in press).

5. Numerical examples

5.1. Grain crushing in cataclastic shear

We use the nonlocal model in the preceding section to study the localisation due to grain crushing in fault gouge (Fig. 3). While several studies, both numerical based (e.g. Shi et al., 2008; Nguyen and Einav, 2009a) and experimental based (e.g. Reches and Dewers, 2005; Chester et al., 2005; Pittarello et al., 2008), have focused the attention on the material behaviour within the cataclasite zone to study the issues of earthquake energy partition, it is the behaviour of an infinite cataclasite layer that will be simulated here using the nonlocal breakage model described in the preceding sections. A new boundary value problem for the cataclasite zone (Fig. 3) will be formulated, taking advantage of the structure and dimension of the fault to derive simplified equilibrium equations. Ignoring body force and inertia effects, the 2D equilibrium equations can be written as:

$$\frac{\partial \sigma_x}{\partial x}+\frac{\partial \tau_{xy}}{\partial y}=0 \quad \text{and} \quad \frac{\partial \tau_{xy}}{\partial x}+\frac{\partial \sigma_y}{\partial y}=0 \tag{45}$$

Further assuming that the variation in the stress condition along the fault line is negligible, and also the thickness of the fault layer is very small compared to its length (Fig. 3), we have the following constraints for the boundary conditions in the horizontal direction (along the fault line):

$$\varepsilon_x=\varepsilon_z=0 \tag{46a}$$

$$\frac{\partial \sigma_x}{\partial x}=0 \quad \text{and} \quad \frac{\partial \tau_{xy}}{\partial x}=0 \tag{46b}$$

We note that Eq. (46b) introduces a strong assumption that simplifies the BVP: one could envisage a solution with a periodic variation of quantities to retain the zero mean. However, while the solution given by Eq. (46b) can potentially suppress some instability modes, the currently simulated mode has the advantage that it can be performed using a simple 1-D Eulerian finite element analysis. The 1-D analysis serves our current purpose of describing the model behaviour in a BVP involving high shearing under pressure. The equilibrium Eq. (45) are then separated purely for the vertical direction:

$$\frac{\partial \tau_{xy}}{\partial y}=0 \quad \text{and} \quad \frac{\partial \sigma_y}{\partial y}=0 \tag{47}$$

The above equations can be solved numerically using 1D finite elements. It should be noted in this case that the stress tensor is still that in 2D plane strain; its time variation is governed by the constitutive behaviour of the model under shearing at constant vertical stress σ_y. Only the spatial variations of σ_x and τ_{xy} in the horizontal direction are zero. The relation between τ_{xy} and σ_y is not seen directly via Eq. (47), but arises from the relevant coupling in the constitutive equations. This way of forming the BVP for an infinite layer is different from that in studies by Tejchman and Gudehus (2001) and Tejchman and Bauer (2004) in which boundary conditions were imposed to a 2D granular layer to simulate its infinite condition.

In our numerical simulation, the material in the cataclasite zone is first subjected to a certain isotropic pressure p_0 corresponding to the depth of the fault. The shearing phase is then carried out under isochoric condition. We use the following material parameters in the numerical simulation: shear modulus $G=5$ GPa; bulk modulus $K=7.5$ GPa; $E_c=0.486$ MPa (corresponding to crushing pressure $p_c=90$ MPa); $M=1.5$; and $\omega=45^o$. Furthermore, the initial pressure is $p_0=70$ MPa and the index property is assumed $\vartheta=0.9$. The localisation is triggered by weakening an element in the middle of the layer, using only 90% of the crushing pressure. The averaging scheme is based on the bell-shaped weighting function of the form:

$$g(\|\mathbf{y}-\mathbf{x}\|)=g(r)=\begin{cases}0 & \text{if } r>R\\ \left(1-\frac{r^2}{R^2}\right)^2 & \text{if } r\leqslant R\end{cases} \tag{48}$$

The spatial parameter in this case is the nonlocal interaction radius R ($R=1.7$ mm in our numerical simulations), which controls the spatial interactions between material points. In this case V_d (Eqs. (25) and (26)) at a material point $\mathbf{x}$ is a sphere of radius R.

The modelled cataclasite zone is of 36 mm thickness, which is comparable to values reported in Chester et al. (2005), and used in DEM simulation by Guo and Morgan (2007). Due to symmetry, only half of the zone is modelled. During the numerical simulation,

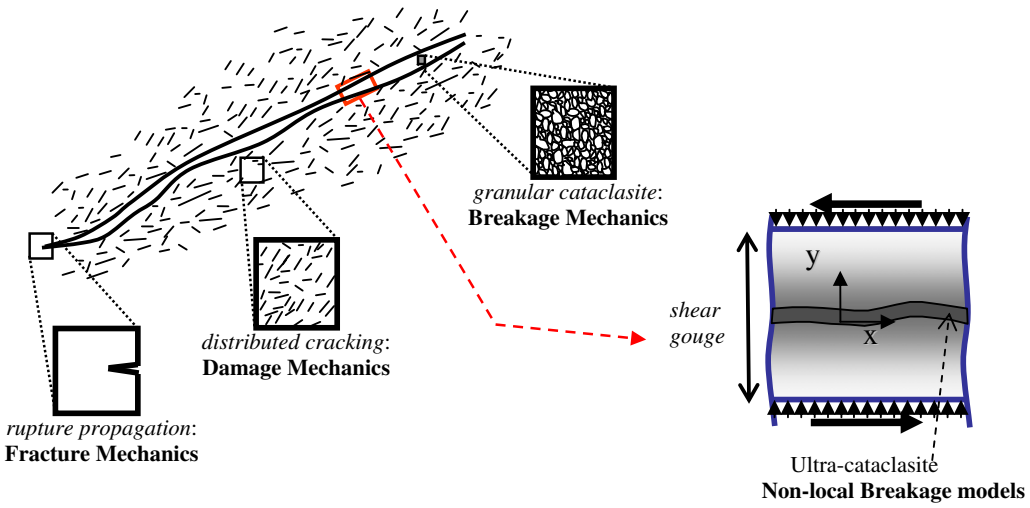

Fig. 3. Modelling grain crushing in cataclasis.

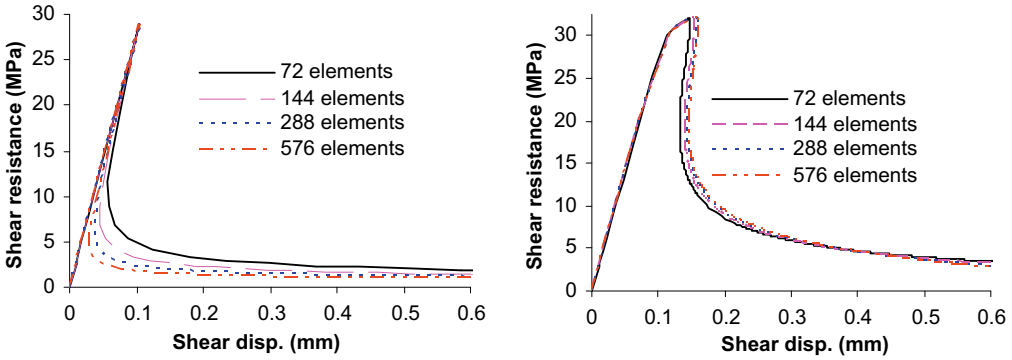

(a): Local breakage model. (b): Nonlocal breakage model.

Fig. 4. Mobilized shear resistance vs. shear displacement.

while the element behaviour evolves during the shearing process, the coordinates of all finite elements are unchanged, representing the flow of the material through a fixed frame. Different finite element meshes are used to illustrate the mesh-independence of the numerical results (Fig. 4b), and highlights the insensitivity of the nonlocal formulation to mesh size alterations in comparison with the local model.

The evolution of the mean grain size of the material in cataclasite zone can be calculated directly using the evolving breakage variable B. In doing that, we assume power law *gsd*'s for both the initial and ultimate conditions:

$$g_i(D) = (3-\alpha_i)\frac{D^{2-\alpha_i}}{D_M^{3-\alpha_i}} \tag{49}$$

where i stands for "u" (ultimate) or "0" (initial). We use an ultimate fractal dimension of $\alpha_u = 2.8$ and set α_0 according to the prescribed value $\vartheta = 0.9$. Using Eq. (3), the mean evolving grain size $\overline{D}$ is:

$$\begin{aligned}\overline{D} &= \int_0^{D_M} Dg(D)dD \\ &= (1-B)\int_0^{D_M} Dg_0(D)dD + B\int_0^{D_M} Dg_u(D)dD \\ &= (1-B)\overline{D}_0 + B\overline{D}_u\end{aligned} \tag{50}$$

where $\overline{D}_0$ and $\overline{D}_u$ are the mean grain sizes at the initial and ultimate conditions, respectively; and the maximum grain size D_M is assumed constant throughout the deformations: $D_M = 0.5$ mm. Fig. 5 plots the evolving mean grain size during the shearing process.

From Fig. 5a, it can be seen that the size of core of the cataclasite layer, i.e., the size of the ultra-cataclasite zone, is unchanged beyond a certain shear level. The size of this core in this example is about $2R$. Inside this core, the grains are continuously crushed towards the ultimate grain size (Fig. 4a and b), while the material outsize the core is only crushed during early stage of the shearing process; then it is unloaded elastically and does not involve cataclastic deformation. The rate of crushing in the core is however decreasing (Fig. 5b) over the time. In other words the material gradually becomes harder to break.

The intrinsic link between the breakage variable and the underlying evolving *gsd* is useful for calculating the permeability reduction of the material within the cataclasite zone (Nguyen and Einav, 2009a). We note that under undrained loading condition, there are no volumetric changes and hence the change of the permeability is caused only by the increase of surface areas of particles, due to the particle crushing process. With the mean grain size decreasing we can see (Fig. 5) that the core of the cataclasite zone in this case acts as a barrier for crossing fluid flow as the shearing progresses.

5.2. Biaxial compression

Numerical simulations of grain crushing in undrained biaxial tests are presented in this section. Similar experimental (Mokni and Desrues, 1998) and numerical studies (Tejchman and Gudehus, 2001; Marcher and Vermeer, 2001; Maier, 2003, 2004; Tejchman, 2004a,b) of granular samples in undrained biaxial loading can be found in the literature. However, they were either for non-crushable granular material (Mokni and Desrues, 1998; Tejchman and Gudehus, 2001; Maier, 2003, 2004; Tejchman, 2004a,b) or using a model without an intrinsic link between the macroscopic (internal) variable and the crushing process at micro (or meso) level (e.g.

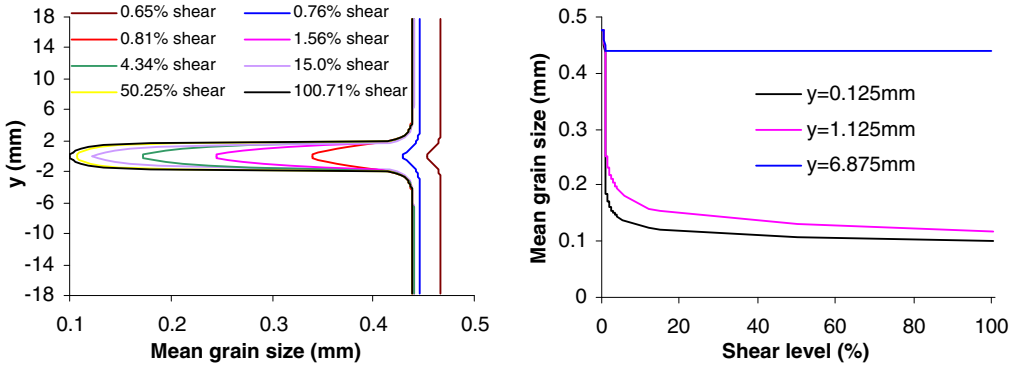

(a): Profile evolution. (b): At different locations.

Fig. 5. Evolution of mean grain size.

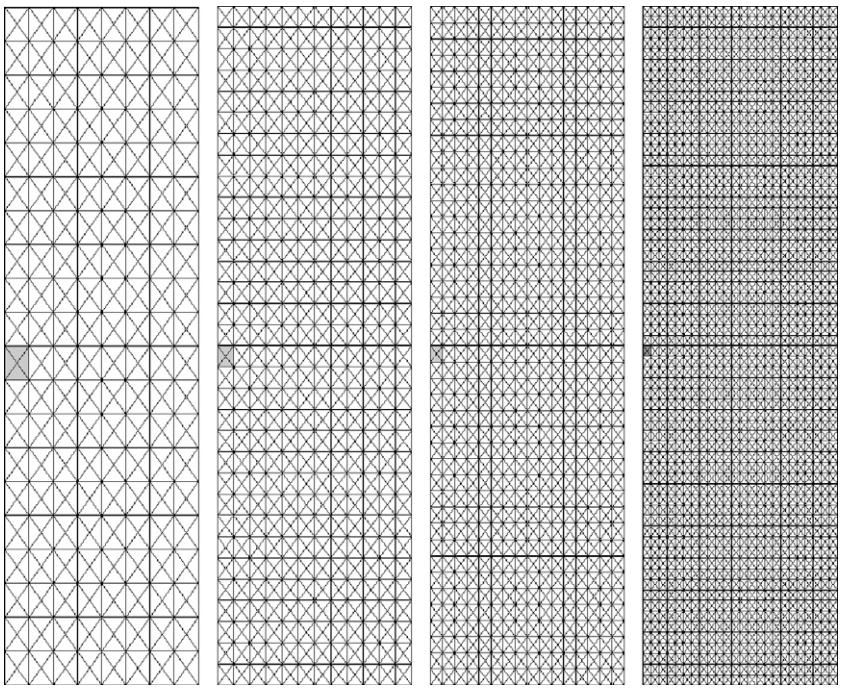

Fig. 6. Finite element meshes.

Daouadji et al., 2001). Here, the nonlocal breakage model presented in Section 2 will be used.

We consider a sand sample (40×140 mm) initially loaded isotropically to a pressure p_0 and then subjected to vertical compression (Fig. 6); this resembles the experimental procedure in Mokni and Desrues (1998). During the course of loading, the lateral stress is kept constant. The sample is assumed to be in plane strain condition, as can be seen in experimental and numerical studies in the literature (e.g. Mokni and Desrues, 1998; Maier, 2003; Tejchman, 2004a,b). To trigger the localisation, a zone (of the size of a quadrilateral element) with lower crushing pressure p_c is introduced to the sample (Fig. 6). The numerical simulations in undrained condition use different meshes of quadrilateral finite elements (Fig. 6). Each quadrilateral element in turn consists of four constant strain triangular elements to avoid volumetric locking (Nagtegaal et al., 1974; Tejchman, 2004a,b). To avoid updating the topological connections of material points for nonlocal averaging, which is very computationally time consuming and requires an effective algorithm, small strain condition is assumed, e.g. the deformation is not taken into account when forming the element stiffness matrix. For the boundary conditions, the bottom of the sample is fixed in the vertical direction, while vertical displacements are incrementally prescribed to nodes at the top of the sample. Zero horizontal movement is also prescribed to the node in the middle of the top to avoid lateral instability. The following model parameters were used: shear modulus $G = 150$ MPa; bulk modulus $K = 300$ MPa; $E_c = 0.3$ MPa (corresponding to crushing pressure $p_c \approx 14$ MPa); $M = 1.2; \omega = 0$. The initial pressure p_0 is set to 10 MPa, while the index property of the sample is $\vartheta = 0.9$. The nonlocal weighting function (48) was also used, with interaction radius $R = 7$ mm. To illustrate the distribution of grain sizes within the sample after crushing, we adopt the same initial and ultimate *gsd* functions

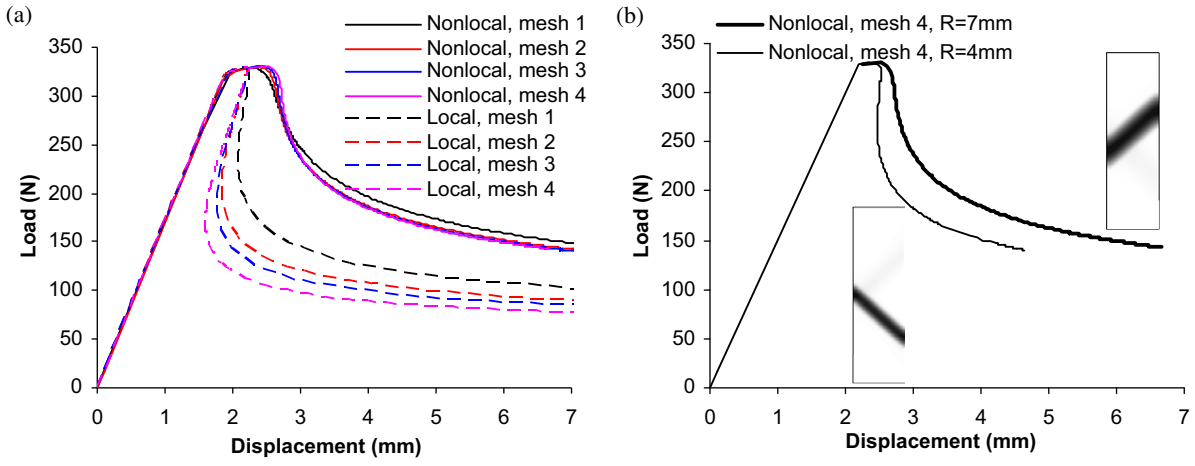

Fig. 7. Load–displacement curves (a) and effect of length parameter on sample responses (b).

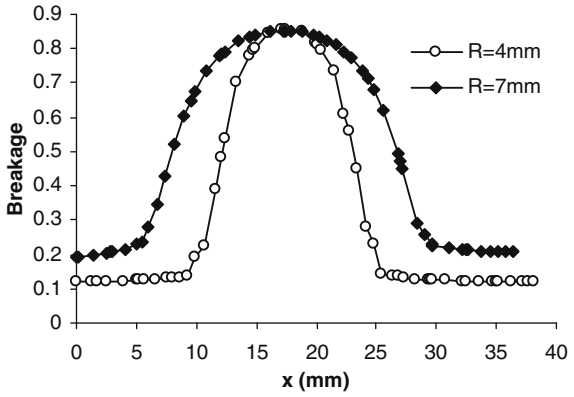

Fig. 8. Effect of the length parameter on shear band width (using mesh 4).

$g_0(d)$ and $g_u(d)$ as described in the preceding example. The maximum grain size in this example is assumed to be $D_M = 1$ mm and is unchanged throughout the shearing phase.

We used GiD (version 9) as the pre- and post-processors for the data and results in this example. The load–displacement curves obtained from both local and nonlocal analysis are shown in Fig. 7a. The nonlocal regularisation effects can be clearly seen in this figure. Provided the finite element discretisation is sufficiently fine (e.g. meshes 2–4), the responses of the numerically simulated sample using different meshes are almost identical. This is not the case for the local analysis, as the deformation tends to localise in a narrow band, the width of which depends on the prescribed size of the finite element. In other words, the localisation bandwidth in local analysis is getting smaller and smaller once the discretisation is refined, resulting in sharper snap-back on the load–displacement curves (Fig. 7a).

It can be seen that different spatial parameters used for the nonlocal model gives different sample responses (Fig. 7b) and different widths of the localisation zone (Fig. 8); this was also numerically observed in Tejchman (2004a). The relationship between local and spatial parameters, along with details on the energy dissipation in grain crushing, should be sorted out to obtain a model that always predicts a unique response with respect to changes of spatial parameter. This is however out of the scope of this study.

The effect of $M = q_u/p_u$, the ratio between the ultimate shear stress q_u and ultimate volumetric stress p_u at failure, on the sample responses can be seen in Fig. 9a. For higher values of M, the material is allowed to take higher shear stress for a given pressure, resulting in higher peak load of the sample. On the other hand, different responses of the sample can also be observed when we change the initial pressure p_0 (Fig. 9b).

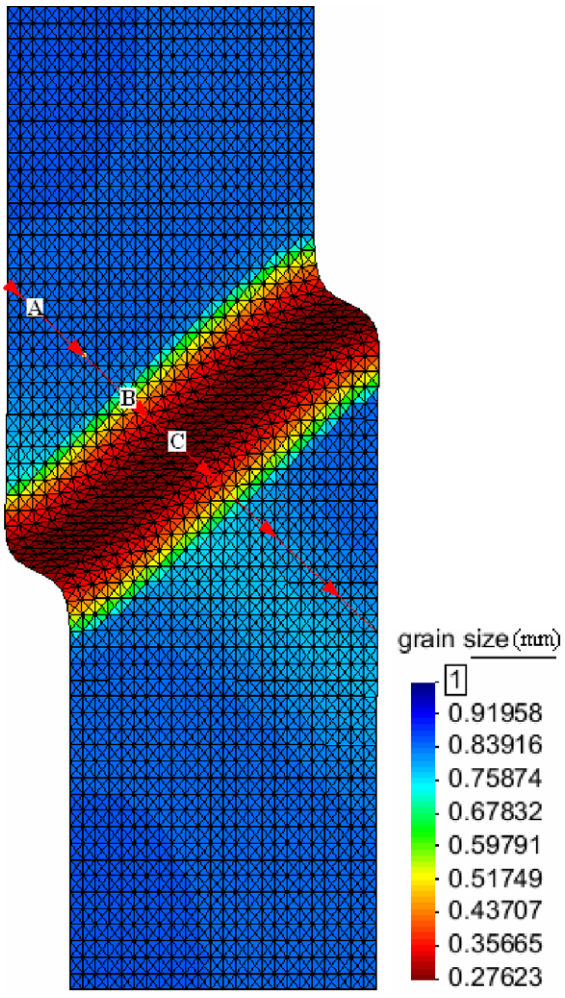

Fig. 10. Deformation and mean *gsd* (mesh 4; magnification factor of 1.5; at 6.66 mm vertical prescribed displacement).

It is interesting to see in Fig. 10 the distribution of the mean grain size within the sample, after severe crushing in localisation band has occurred. The profile of the mean grain size, along with

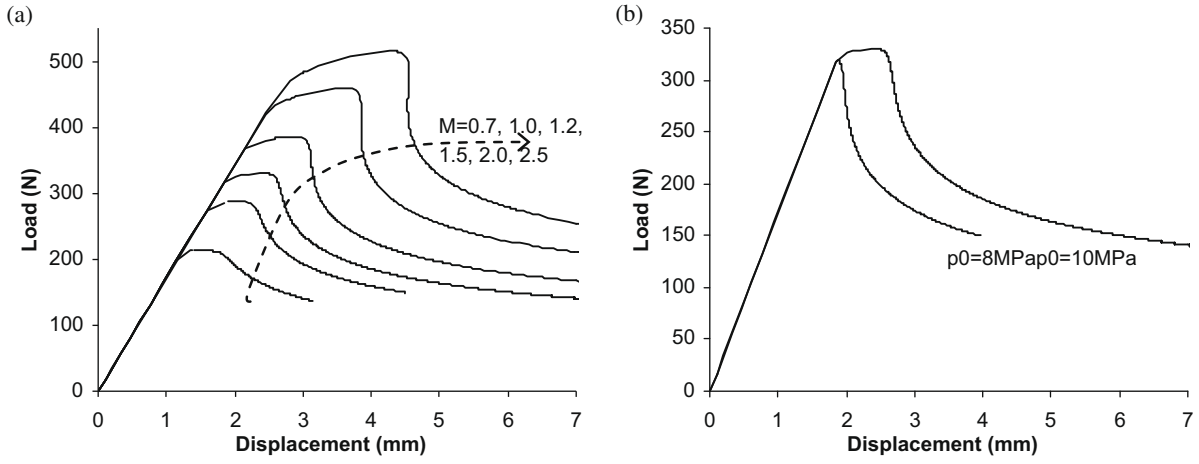

Fig. 9. Effects of (a) $M = q_u/p_u$ and (b) initial pressure p_0 on the sample responses (using mesh 3).

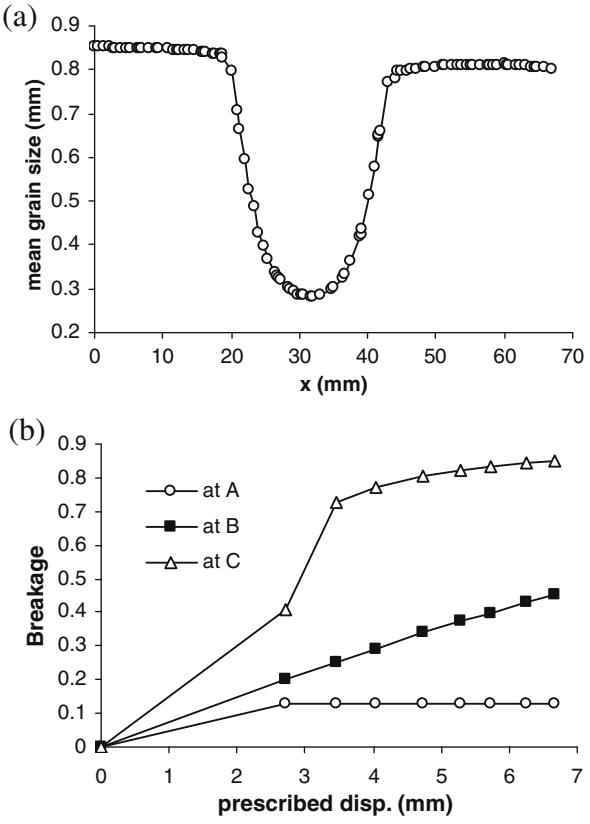

Fig. 11. (a) Mean grain size profile across the localisation band; (b) breakage evolution at points A, B, C (see Fig. 10).

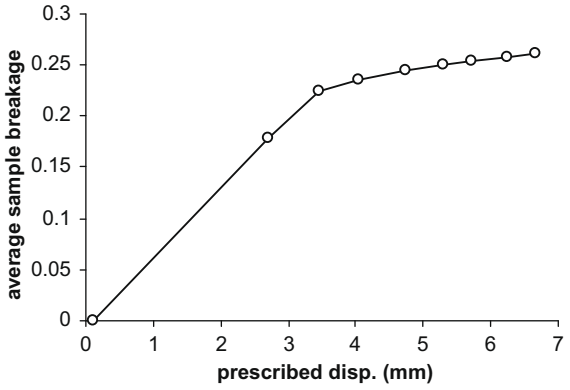

Fig. 12. Averaged breakage (over the whole sample) vs. prescribed displacement.

the breakage evolutions at different spatial points, is also plotted (Fig. 11), highlighting the crushing process within the sample. We can see that at early stage of the shearing process, grain crushing occurs over the whole sample, corresponding to the hardening phase in the load–displacement curves. During this phase, the mean breakage averaged over the whole sample is increasing rapidly with increasing prescribed vertical displacement (Fig. 11b). The localisation will then be activated when the material in weakened elements enter its softening phase. During the localisation phase the rate of increment of the average sample breakage (the spatial average of breakage) is gradually slowing down (Fig. 12), because only the material within the localisation band (e.g. points B and C in Figs. 10 and 11b) is crushing towards the ultimate *gsd*, while other elements outside the localisation band are unloaded elastically (e.g. point A in Figs. 10 and 11b). It can be expected that localisation of grain crushing prevents the average sample breakage to ever reach unity.

6. Discussions and conclusions

The nonlocal regularisation applied to a breakage model (Einav, 2007c) was numerically shown to stabilise the model behaviour and to bring well-posedness to BVPs involving softening due to grain crushing. We showed the capability of the regularised model in capturing the evolving *gsd* of the materials in shearing processes at high pressure. The obtained numerical solutions are mesh-independent, and the localisation of deformation into non-zero volume is numerically observed. There are, however, several aspects of the nonlocal regularisation of constitutive models based on breakage mechanics that need to be further investigated. The localisation analysis for the nonlocal breakage model will be carried out in the next step to obtain rigorous mathematical aspects of the nonlocal regularisation. The formulation of a consistent nonlocal thermodynamic framework for breakage model is another aspect that requires further study. In addition, one should pay attention to the link between the spatial length and the *gsd*, critical to modelling evolving ultra-cataclasite zone in fault gouge. In this paper, for the sake of simplicity, it was assumed that the spatial length (nonlocal radius) does not evolve with the change of the *gsd*. However, due to crushing the *gsd* is shifting towards its ultimate distribution, reducing the critical size of the RVE of the granular ensemble. Since this critical size of the RVE is related to the length scale of the nonlocal continuum model, an evolving length scale is therefore required. The formulation of a consistent thermodynamics-based nonlocal breakage model with an evolving length scale is expected to be a challenging task in the next step of model development.

Acknowledgements

This research was supported under Australian Research Council's Discovery Projects funding scheme (Project No. DP0774006). Financial support to the first author, through the University of Sydney Postdoctoral Fellowship, and the Bridging Support Grant, is gratefully acknowledged.

References

Borino, G., Failla, B., Parrinello, F., 2003. A symmetric nonlocal damage theory. International Journal of Solids and Structure 40, 3621–3645.
Chester, J.S., Chester, F.M., Kronenberg, A.K., 2005. Fracture surface energy of the Punchbowl fault, San Andreas system. Nature 437 (7055), 133–136.
Collins, I.F., Einav, I., 2005. On the validity of elastic/plastic decompositions in soil mechanics. In: Tanaka, T., Okayasu, T. (Eds.), Proceeding of Symposium on Elastoplasticity. Kyushu University, Japan, pp. 193–200.
Crisfield, M.A., 1997. Non-Linear Finite Element Analysis of Solids and Structures, vols. 1 and 2. Wiley, New York.
Crook, A.J.L., Willson, S.M., Yu, J.G., Owen, D.R.J., 2006. Predictive modelling of structure evolution in sandbox experiments. Journal of Structural Geology 28, 729–744.
Daouadji, A., Hicher, P.-Y., Rahma, A., 2001. An elastoplastic model for granular materials taking into account grain breakage. European Journal of Mechanics A/Solids 20, 113–137.
Einav, I., 2007a. Breakage mechanics – Part I: Theory. Journal of the Mechanics and Physics of Solids 55 (6), 1274–1297.
Einav, I., 2007b. Breakage mechanics – Part II: Modelling granular materials. Journal of the Mechanics and Physics of Solids 55 (6), 1298–1320.
Einav, I., 2007c. Fracture propagation in brittle granular matter. Proceedings of the Royal Society A: Mathematical. Physical and Engineering Sciences 463 (2087), 3021–3035.
Einav, I., Nguyen, G.D., 2009. Cataclastic and ultra-cataclastic shear using breakage mechanics. Batsheva De Rothschild Seminar on "Shear Physics at the Meso-scale in Earthquake and Landslide Mechanics". Ein Gedi, the Dead Sea Valley, Israel, 26–30 January 2009.
GiD version 9.0, The personal pre- and post-processor. International Center for Numerical Methods in Engineering. Barcelona, Spain.

Guo, Y., Morgan, J.K., 2007. Fault gouge evolution and its dependence on normal stress and rock strength – results of discrete element simulations: gouge zone properties. Journal of Geophysical Research 112, B10403.
Houlsby, G.T., Puzrin, A.M., 2000. A thermomechanical framework for constitutive models for rate-independent dissipative materials. International Journal of Plasticity 16, 1017–1047.
Jirásek, M., 1998. Nonlocal models for damage and fracture: comparison of approaches. International Journal of Solids and Structures 35 (31–32), 4133–4145.
Jirásek, M., Bazant, Z.P., 2002. Inelastic Analysis of Structures. John Wiley & Sons Ltd..
Lemaitre, J., 1971. Evaluation of dissipation and damage in metals. In: Proceedings of the I.C.M, vol. 1. Kyoto, Japan.
Lemaitre, J., 1992. A Course on Damage Mechanics. Springer Verlag.
Maier, T., 2003. Nonlocal modelling of softening in hypoplasticity. Computers and Geotechnics 30, 599–610.
Maier, T., 2004. Comparison of non-local and polar modelling of softening in hypoplasticity. International Journal for Numerical and Analytical Methods in Geomechanics 28, 251–268.
Marcher, T., Vermeer, P.A., 2001. Macromodelling of softening in non-cohesive soils. In: Vermeer, P.A., Diebels, S., Ehlers, W., Herrmann, H.J., Luding, S., Ramm, E. (Eds.), Continuous and Discontinuous Modelling of Cohesive-Frictional Materials, Lecture Notes in Physics, vol. 568, pp. 89–110.
Mokni, M., Desrues, J., 1998. Strain localisation measurements in undrained plane-strain biaxial tests on Hostun RF sand. Mechanics of Cohesive-Frictional Materials 4, 419–441.
Nagtegaal, J.C., Parks, D.M., Rice, J.R., 1974. on numerically accurate finite element solutions in the fully plastic range. Computer Methods in Applied Mechanics and Engineering 4, 153–177.
Neilsen, M.K., Schreyer, H.L., 1993. Bifurcation in elastic–plastic materials. International Journal of Solids and Structures 30 (4), 521–544.
Nguyen, G.D., Einav, I., 2009a. The energetics of cataclasis based on breakage mechanics. Pure and Applied Geophysics 166 (10–11), 1693–1724.
Nguyen, G.D., Einav, I., in press. A stress return algorithm for nonlocal constitutive models of softening materials. International Journal for Numerical Methods in Engineering. doi:10.1002/nme.2790.
Nguyen, G.D., Einav, I., Vardoulakis, I., 2008. Modelling high pressure shear using breakage mechanics. In: XXII International Congress of Theoretical and Applied Mechanics. Adelaide, Australia, 24–30 August 2008.
Ord, A., Hobbs, B., Regenauer-Lieb, K., 2007. Shear band emergence in granular materials – a numerical study. International Journal for Numerical and Analytical Methods in Geomechanics 31, 373–393.
Pijaudier-Cabot, G., Bazant, Z.P., 1987. Nonlocal damage theory. ASCE Journal of Engineering Mechanics 113 (10), 1512–1533.
Pijaudier-Cabot, G., Benallal, A., 1993. Strain localization and bifurcation in a nonlocal continuum. International Journal of Solids and Structure 30 (13), 1761–1775.
Pittarello, L., Di Toro, G., Bizzarri, A., Pennacchioni, G., Hadizadeh, J., Cocco, M., 2008. Energy partitioning during seismic slip in pseudotachylyte-bearing faults (Gole Larghe Fault, Adamello, Italy). Earth and Planetary Science Letters 269 (1–2), 131–139.
Reches, Z., Dewers, T.A., 2005. Gouge formation by dynamic pulverization during earthquake rupture. Earth and Planetary Science Letters 235 (1–2), 361–374.
Rubin, M.B., 2001. Physical reasons for abandoning plastic deformation measures in plasticity and viscoplasticity theory. Archives of Mechanics 53 (4–5), 519–539.
Shi, Z., Ben-Zion, Y., Needleman, A., 2008. Properties of dynamic rupture and energy partition in a solid with a frictional interface. Journal of the Mechanics and Physics of Solids 56, 5–24.
Sluys, L., de Borst, R., Muhlhaus, H.-B., 1993. Wave propagation, localization and dispersion in a gradient-dependent medium. International Journal of Solids and Structures 30 (9), 1153–1171.
Tejchman, J., 2004a. Comparative FE-studies of shear localisations in granular bodies within a polar and non-local hypoplasticity. Mechanics Research Communication 31, 341–354.
Tejchman, J., 2004b. Influence of a characteristic length on shear zone formation in hypoplasticity with different enhancements. Computers and Geotechnics 31, 595–611.
Tejchman, J., Bauer, E., 2004. Effect of cyclic shearing in shear localisation in granular bodies. Granular Matter 5, 201–212.
Tejchman, J., Gorski, J., 2008. Computations of size effects in granular bodies within micro-polar hypoplasticity during plane strain compression. International Journal of Solids and Structures 45, 1546–1569.
Tejchman, J., Gudehus, G., 2001. Shearing of a narrow granular layer with polar quantities. International Journal for Numerical and Analytical Methods in Engineering 25, 1–28.
Ziegler, H., 1983. An Introduction to Thermomechanics, second ed. North Holland, Amsterdam.